Emergent Materials (2025) 8:6791–6806
https://doi.org/10.1007/s42247-025-01108-6

ORIGINAL ARTICLE

Effect of filament humidity on the properties of material extrusion 3D-printed acrylonitrile butadiene styrene/hexagonal boron nitride composites

László Lendvai[1,2] · Sándor Kálmán Jakab[1,2] · Imre Fekete[1,2] · Daniele Rigotti[3] · Alessandro Pegoretti[3]

Received: 12 February 2025 / Accepted: 29 April 2025 / Published online: 15 May 2025

Abstract

This study investigates the effect of filament moisture content on material extrusion (MEX) 3D-printed composites using acrylonitrile butadiene styrene (ABS) as the polymer matrix and 0–10 vol% hexagonal boron nitride (BN) as reinforcement. ABS/BN composites were prepared through batchwise compounding and extruded into MEX-suitable filaments. The filaments were conditioned at 30 °C and 10% or 90% relative humidity (RH) before/during direct feeding into the 3D printer. Specimens were fabricated with raster angles parallel (0°) and perpendicular (90°) to their length. Micro- and macrostructural analyses using scanning electron microscopy and computed tomography revealed intensive void formation, especially in BN-filled composites 3D-printed from humid filaments. This was attributed to BN acting as a physical barrier, hindering the outgassing of evaporated water during 3D printing. Mechanical properties were evaluated using tensile and Charpy impact tests. Based on the tensile test results, neat ABS was the least sensitive to filament moisture, with tensile strength at 0° raster angle dropping from 40.5 MPa to 36.7 MPa as storage RH was increased from 10 to 90%. For composites with 10 vol% BN loading, tensile strength dropped from 34.1 MPa to 22.3 MPa. Charpy impact strength exhibited similar reductions, ascribed to the porous structure of the BN-filled composites caused by the evaporated moisture. Thermal conductivity was also examined, showing slightly superior performance for samples 3D-printed from filaments stored in less humid conditions. For unfilled ABS, the conductivity slightly decreased from 0.188 to 0.185 W/mK, while for 10 vol% BN-filled composite, it dropped from 0.778 to 0.617 W/mK.

Keywords Acrylonitrile butadiene styrene · Hexagonal Boron nitride · Material extrusion · Fused deposition modeling · Fused filament fabrication · Additive manufacturing · Filament · Humidity

1 Introduction

Recently, additive manufacturing (AM), also known as 3D printing, has emerged as a revolutionary and attractive manufacturing process, as it allows flexible engineering design using CAD software without the need for costly molds [1].

Various AM techniques share a common characteristic of building the desired objects by adding material in successive layers [2]. Material extrusion (MEX), often denoted as fused deposition modeling (FDM) or fused filament fabrication (FFF), is the most widely used method among AM processing techniques [3, 4]. MEX 3D printers produce objects using thermoplastic feedstock in the form of a filament, which is melted and then deposited onto a build platform through a heated nozzle that moves along a horizontal, pre-specified pathway defined by a G-code. Once a layer is completed, the build platform is lowered by one unit to continue with the next layer [5]. The popularity of MEX can be ascribed to its simplicity, low cost, and the range of materials that can be processed with it.

MEX 3D printers are generally compatible with a wide variety of polymers. Among these, the most commonly

✉ László Lendvai
lendvai.laszlo@sze.hu

1 Department of Materials Science and Engineering, Széchenyi István University, Egyetem tér 1, Győr 9026, Hungary

2 Sustainable Polymer Engineering Research Group, Széchenyi István University, Egyetem tér 1, Győr 9026, Hungary

3 Department of Industrial Engineering, University of Trento, Trento 38123, Italy

used ones are acrylonitrile butadiene styrene (ABS) and poly(lactic acid) (PLA) due to their favorable rheological and thermal properties, as well as ease of processing. However, glycol-modified poly(ethylene terephthalate) (PET-G), thermoplastic polyurethane (TPU), polyamide 6 (PA6), polyether-ether-ketone (PEEK), and polycaprolactone (PCL) are also regarded as commonly used feedstocks [6–10]. In addition to raw plastics, an increasing number of studies are focused on employing polymer-based multicomponent materials, i.e., blends and composites, for 3D printing applications in order to obtain products with superior properties compared to their unmodified counterparts. One potential field where the benefits of additive manufacturing can be effectively exploited is in the processing of thermally conductive polymeric materials typically used in electrical and electronic applications, where heat transfer efficiency is the bottleneck in thermal management [11, 12]. Corresponding devices, typically owning a high energy density, include integrated electronic packaging, light-emitting diodes (LEDs), batteries, 5G devices, and microchips [13–16]. For these applications, effective heat dissipation is a crucial requirement to maintain good performance, service lifetime, and stable operation. Products with enhanced thermal management can be achieved through two primary means: (i) increasing the surface area via geometry and topology optimization or (ii) improving the thermal conductivity of the material used for the production of the heat sink attached to the electronic device [17]. 3D printing is an ideal technique in both respects, as it allows a flexible geometry design, and the polymeric feedstock can also be property-tailored with suitable additives to achieve effective heat dissipation. When it comes to thermally conductive polymer composites, the three major groups of additives to be considered are carbonaceous, metallic, and ceramic particles [18–20]; however, depending on the application, some of the listed filler types can be less ideal than others. Specifically, where good electrical conductivity could compromise safety conditions, metals, and carbon-based additives should be avoided. Hence, ceramic particles are the obvious choice for such purposes. In the literature, a wide variety of ceramic fillers have been studied to improve the thermal conductivity of polymers along with maintaining their excellent electrical resistivity as well. These include aluminum oxide (Al_2O_3) [21, 22], magnesium oxide (MgO) [23], aluminum nitride (AlN) [24–26], silicon carbide (SiC) [27], silicon oxide (SiO_2) [28], and boron nitride (BN) [13, 29–31]. Hexagonal BN, also referred to as "white graphite", has attracted much attention over the last several years. It exhibits a layered structure similar to that of graphite [32, 33]. In addition to its excellent thermal conductivity, it possesses decent electrical resistivity, relatively low density, and high thermal stability, and it also has a strongly hydrophobic nature [34].

When it comes to the MEX 3D printing-based fabrication of various engineering products, there are several process variables that need to be optimized in order to obtain quality parts. These include bead width, layer thickness, nozzle and build platform temperature, infill pattern, raster angle, build orientation, extrusion rate, and other factors, all of which influence the resulting product's mechanical, physical, and geometrical features. To date, a large number of studies have focused on the importance of the listed parameters with regard to the resulting quality of the 3D-printed objects [35–38]. Examples of works focusing on this topic include the research of [39], which investigated the effect of different infill patterns (line, triangle, and concentric), infill densities (75, 80, and 85%), and layer thicknesses (100, 200, and 300 μm) on the mechanical properties of 3D-printed parts using ABS as the feedstock. The authors found the most advantageous results when a concentric infill pattern, along with 80% infill density and 100 μm layer thickness was applied. Chacón et al. [40] examined the changes in the mechanical properties of PLA samples by varying the feed rate (1.9, 4.8, and 7.7 mm^3/sec), build orientation (on-edge, flat, and upright), and layer thickness (0.06, 0.12, 0.18, and 0.24 mm). Their study revealed that the ductility of the 3D-printed objects decreases as layer thickness and feed rate increase. It was also found that variations in mechanical properties as a function of feed rate and layer thickness were not significant for on-edge and flat orientations. Ulkir et al. [41] analyzed the impact of nozzle temperature settings on the dimensional accuracy and mechanical properties of samples fabricated with ABS filaments. The authors increased the nozzle temperature from 220 °C to 270 °C in increments of 10 °C. It was found that dimensional accuracy deteriorates with increasing nozzle temperature, along with decreasing density and strength, which were attributed to the lower viscosity of the polymer melt.

As highlighted above, the widespread use of MEX-based 3D printing has garnered considerable interest from both industrial and academic fields, leading to a proliferation of studies focused on understanding the effects of factors influencing the properties of fabricated parts. However, further parameters equally important as those previously described have received less emphasis until recently. One such parameter is the moisture content of the feedstock, which can greatly vary depending on the environmental conditions, including temperature and relative humidity (RH). Industrial players involved in polymer processing are well aware that plastics should be dried before melt processing in order to avoid molecular degradation, the formation of surface defects, and internal voids. Additive manufacturing is being increasingly utilized across diverse fields, including

medicine, architecture, fashion, electronics, and even by individual users, where expertise in polymer science cannot always be expected, often leading to the neglect of feedstock drying. This underlines the necessity of understanding the effect of the environmental conditions where the filament is stored on the quality of the products fabricated from it so this can be considered during product design. Despite its importance, only a limited number of studies have been published to date, as summarized below.

In a research conducted by Fang et al. [42], a desktop MEX 3D printer was placed in an environmental control system, along with the polycarbonate (PC) filament that was used for specimen fabrication. During the experiments, the temperature was varied from 30 °C to 90 °C, while the RH ranged from 10 to 70%. As ambient humidity increased, the moisture absorbed by the PC filament also increased. It was found that absorbed moisture significantly influences the melt viscosity of the polymer due to water being a low-molecular weight substance that plasticizes the plastic. Consequently, the quality of the 3D-printed objects was also greatly affected, resulting in reduced strength in both longitudinal and transverse directions. Hamrol and his colleagues [43] analyzed the strength and dimensional accuracy of 3D-printed products by varying the ABS filament moisture content between 0.17% and 0.75%. The authors reported an overall decrease in strength of 25% and an increase in sample thickness of 10% at higher filament moisture. Halidi and Abdullah [44] highlighted a further issue related to excess moisture: filament swelling, which can lead to nozzle blockage and compromise the printing process. The authors reported a 5% increase in filament diameter when it was stored in a high-moisture environment for an extended period. In addition to nozzle clogging, it is important to consider that the actual volume of plastic extruded through the nozzle is less than the input volume, as the water absorbed by the filament evaporates at the processing temperature, which far exceeds its boiling point. Furthermore, it was underlined that moisture also decreases the glass transition temperature of ABS, which can lead to inconsistent printing performance. Laumann et al. [45] conducted a comprehensive analysis on the effect of feedstock moisture content on the adhesion between printed beads and the build platform using PLA, polyvinyl alcohol (PVA), and PA6 filaments. The authors found that the moisture content of the printing material could alter the adhesion between the 3D-printed part and the build surface by up to 68%. Whichniarek et al. [46] observed that the mechanical properties of ABS deteriorate when filament moisture content increases from 0.1 to 0.6%. In their study, the authors tested several methods in order to compensate for this loss, finding that reducing the layer thickness was the most effective approach.

As highlighted above, recent literature has identified filament moisture content as a valid and significant disturbance in MEX 3D printing, with considerable influence on printing quality that warrants further investigation. Obviously, the optimal strategy to prevent the negative effects from moisture would be to properly store the feedstock or dry it before processing; however, this is not always feasible or economically viable. Previous studies dealing with the effect of filament moisture content on the printing quality have exclusively focused on raw, unfilled polymeric materials. The increasingly widespread use of polymer-based composites in MEX 3D printing justifies extending this research to multicomponent materials as well. Currently, detailed information on this subject is lacking in the available literature. In this regard, BN, a ceramic filler used in plastic products intended for heat sink applications in electronic devices, could be particularly interesting due to its inherently hydrophobic nature, which may help reduce the impact of moisture absorption.

In this study, BN-filled ABS composites were prepared with boron nitride content ranging from 0 to 10 vol%. After melt compounding, the composites were formed into filaments suitable for MEX 3D printing purposes. The ABS/BN filaments were conditioned in environments with significantly different ambient humidity levels (10% and 90%). Specimens were then produced by directly feeding the conditioned filaments into the 3D printer's nozzle in order to analyze the effect of environmental storage conditions on the quality of the 3D-printed objects. The samples were examined for their macrostructure using computed tomography and scanning electron microscopy. Mechanical and thermomechanical properties were analyzed through tensile tests, Charpy impact tests, and dynamic mechanical analyses. Additionally, the thermal conductivity and electrical resistivity of the composites were investigated through the laser flash technique and resistivity measurement.

2 Materials and methods

2.1 Materials

Magnum 3453 ABS, obtained from Trinseo (Wayne, Pennsylvania, USA), was used as the polymer matrix. According to its official datasheet, this ABS grade exhibits a density of 1.05 g/cm^3 and a melt flow rate of 15 g/10 min (10 kg/220 °C). Hexagonal BN (Hebofill 482), obtained from Henze BNP (Lauben, Germany), was introduced as a nanofiller with a density of 1.88 g/cm^3, and its average particle size is reported to be < 30 µm. It is important to note that this latter value refers to the size of BN agglomerates, with the individual particles being much smaller than that. A scanning

electron microscopic image of the BN particles is shown in Fig. 1.

2.2 Filament fabrication

Before processing, both ABS and BN were dried in a ventilated oven at 80 °C for 3 hours to remove their inherent moisture content. The compounding of the components was carried out using a Haake Polylab internal mixer (Vreden, Germany) equipped with a 50 cm^3 kneading chamber, operated at 190 °C and a rotor speed of 60 rpm. The BN was poured into the device after melt masticating ABS for 3 mins. Once both components were introduced into the mixer, compounding continued for an additional 7 mins to achieve a homogenous dispersion. Three samples were prepared in this way with a hexagonal BN content of 0, 5, and 10 vol%, denoted as ABS, ABS_5BN, and ABS_10BN, respectively. The prepared composites were ground with an F.lli Virginio plastic shredder (Gambellara, Italy) into particles of ~3 mm before further processing. Filaments suitable for MEX-based 3D printing (diameter = 1.75 ± 0.05 mm) were obtained by feeding the ground pellets into a 3Devo Precision 450 filament extruder (Utrecht, The Netherlands). The heating zones of the barrel, from feeder to die, were set to 240 °C, 230 °C, 230 °C, and 220 °C, and the rotational speed of the screw was 3.5 rpm.

2.3 3D printing

Before 3D printing, the filaments were stored in an Angelantoni ACS DY110 humidity-controlled chamber (Massa Martana, Italy) for at least seven days in order to stabilize their moisture content. The chamber temperature was maintained at 30 °C, while the RH was set to 10% for the first set of specimens and to 90% for the second set. The storage conditions were preserved during the entire 3D printing process, with the filaments directly fed from the humidification chamber to the 3D printer's nozzle. In order to prevent the filaments from absorbing or dissipating moisture from/to the environment, they were protected by a silicon tube between the test chamber and the 3D printer. A schematic view of the experimental setup is available in a previous work [47]. For specimen fabrication, a Craftbot Plus desktop 3D printer (Budapest, Hungary) was employed. During the printing of the specimens, two linear infill orientations were employed to isolate the mechanical properties along the beads (0°) and perpendicular to them (90°) to better understand the effect of filament storage humidity on the properties. All other printing parameters were kept constant, including a nozzle diameter of 0.4 mm, a nozzle temperature of 260 °C, a build platform temperature of 110 °C, a printing speed of 50 mm/sec, a layer thickness of 0.2 mm, and two shell layers. The G-code for the printer head's toolpath was generated using SuperSlicer software.

2.4 Characterization

The effect of BN-content on the moisture-absorption of ABS was investigated by storing samples in a humidity-controlled environment for an extended period. This measurement was carried out to determine the moisture content of the filaments used for MEX 3D printing purposes. First, the ABS and the ABS/BN composites were dried in a ventilated oven at 60 °C until a constant dry weight was achieved. Subsequently, the samples were placed into the humidity test chamber at a temperature of 30 °C, and a relative humidity of 10% or 90% (identical to the experimental conditions), and their weight gain was registered as a function of storage time. The moisture content (*%M*) was then calculated using Eq. (1).

$$\%M = \frac{M_F - M_I}{M_I} \tag{1}$$

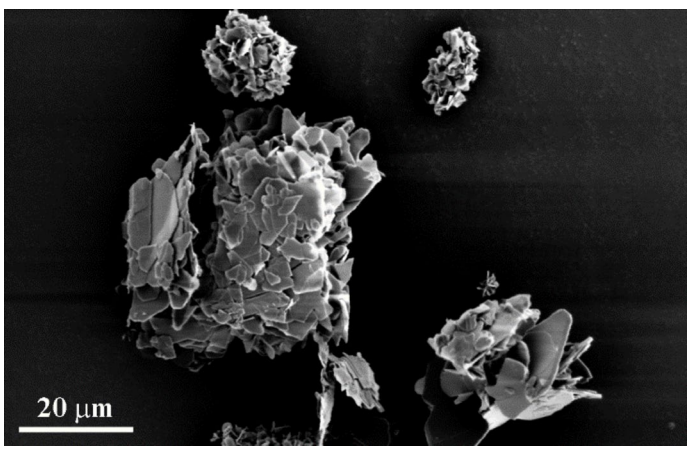

Fig. 1 Scanning electron microscopic image of the hexagonal BN flakes forming agglomerates

where M_I is the initial dry weight of the filaments, and M_F is their weight after a specific storage time inside the humidity test chamber.

The macrostructure of the 3D-printed parts was analyzed by computed tomography (CT), which, among other uses, is an excellent tool to characterize or quantify additively manufactured structures. To reveal the porous or solid structure that may have evolved during 3D-printing, an industrial CT system was employed. For this purpose, a still intact rectangular Charpy specimen was scanned. The CT scanner in these experiments was used at 190 kV and 130 µA accelerating voltage and current, respectively. A 1-megapixel square detector was used to capture 1620 X-ray images during the full revolution of the scan. The CT system was operated in an offset mode that effectively doubles the detector resolution in the horizontal plane, providing a better image resolution. The scan time for one specimen was 45 min, and after reconstruction, a voxel array with a voxel size of 8.02 µm was analyzed. Cross-sections along the building direction (Z axis) and the Y axis of the specimens are presented in the results section.

In order to analyze the microstructure and morphology of the samples, scanning electron microscopy (SEM) was applied. For this purpose, a Hitachi S-3400 N (Tokyo, Japan) microscope at an acceleration voltage of 10 kV was used. The specimens were sputter-coated with gold using a Quorum Emitech SC7620 instrument (Laughton, UK) under a flow of argon to prevent charging.

The tensile properties of the samples were measured in accordance with the ISO 527 standard using an Instron 5582 universal testing machine (Norwood, Massachusetts, USA) equipped with a 10 kN load cell. The specimens used for the tensile tests had a dogbone-shaped geometry corresponding to the 1BA type of ISO 527-2. The clamping distance was 58 mm, and the tensile speed was 1 mm/min until 0.3% deformation, after which it was increased to 5 mm/min.

Charpy impact tests were carried out according to ISO 179 using a Ceast 6545 impact tester (Pianezza, Italy) equipped with a 15 J hammer. The tests were performed with rectangular specimens measuring $4 \times 10 \times 80$ mm^3, and the span length was 62 mm.

Dynamic mechanical analysis (DMA) was conducted using a TA Instruments Q800 apparatus (New Castle, Delaware, USA) equipped with a dual-cantilever clamp. The rectangular samples of $4 \times 10 \times 60$ mm^3 were heated from 40 to 150 °C at a heating rate of 3 °C/min. The frequency was 1 Hz, and the oscillation amplitude was set to 0.02%.

The thermal conductivity of the samples was examined by laser flash analysis (LFA) using a Netzsch LFA 467 Hyperflash (Selb, Germany) apparatus. Cylindrical specimens with 12.7 mm diameter and 3 mm thickness, coated with graphite were used for the test. Five pulses were performed on each specimen. Considering that the different infill orientations are equivalent from the measurement's point of view, only a single type was applied.

The electrical resistivity of the 3D-printed samples was measured using a Keithley 8009 resistivity tester (Cleveland, Ohio, USA) coupled with a Keithley 6517 A high-resistance meter (Cleveland, Ohio, USA). For this purpose, cylindrical specimens of 80 mm diameter and 1 mm thickness were used. To ensure the best contact surface, an ironing step was used during the 3D printing of the top layer of the specimens. Similar to the thermal conductivity test, only a single infill orientation type was applied, as the different orientations were equivalent from the measurement's perspective.

The obtained results, wherever applicable, were evaluated using the one-way analysis of variance (ANOVA) method, followed by Tukey HSD post hoc tests at a significance level of 5% ($p < 0.05$).

The specimens fabricated for the various tests are shown in Fig. 2, along with a schematic representation of the infill orientations used.

3 Results and discussion

3.1 Moisture absorption behavior

As a first step, the neat ABS and ABS/BN composite filaments were characterized for their moisture absorption behavior under the experimental conditions. The percentage of water uptake (*%M*) when stored at 10% and 90% relative humidity is shown in Fig. 3. In all cases, the curves can be divided into two regions: (i) absorption, during which the weight of the specimens gradually increases, and (ii) stabilization, when saturation is reached and the weight remains constant. As expected, the amount of water absorbed by the materials greatly depends on the environmental conditions; in a relatively dry environment (RH = 10%), the maximum water uptake after one week for all specimens was in the range of 0.149–0.161%, while storing at 90% RH resulted in considerably higher maximum water absorption (0.503–0.631%). After conditioning for 168 h, the differences in weight increment were approximately proportional to the BN content of the samples, with the BN-filled samples absorbing less moisture. This can be attributed to the strongly hydrophobic nature of the ceramic particles, indicating that the fillers absorbed little to no water. Furthermore, under both RH conditions, neat ABS always reached saturation first, with its weight stabilizing after 72 h of conditioning. Meanwhile, for the BN-filled samples, it took between 120 and 144 h to achieve a stabilized weight. Accordingly, it can be assumed that the BN platelets acted

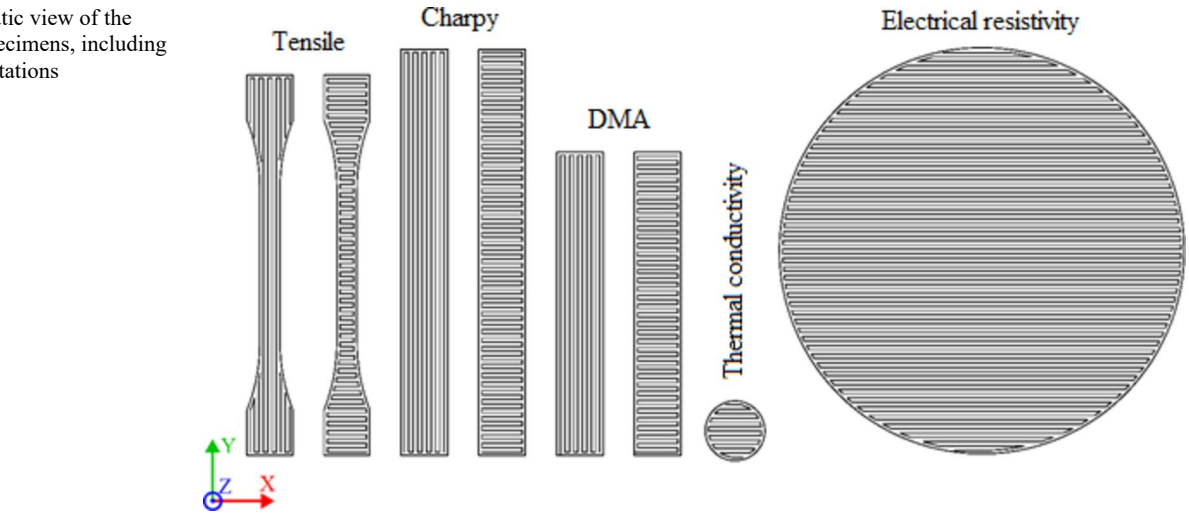

Fig. 2 Schematic view of the 3D-printed specimens, including the infill orientations

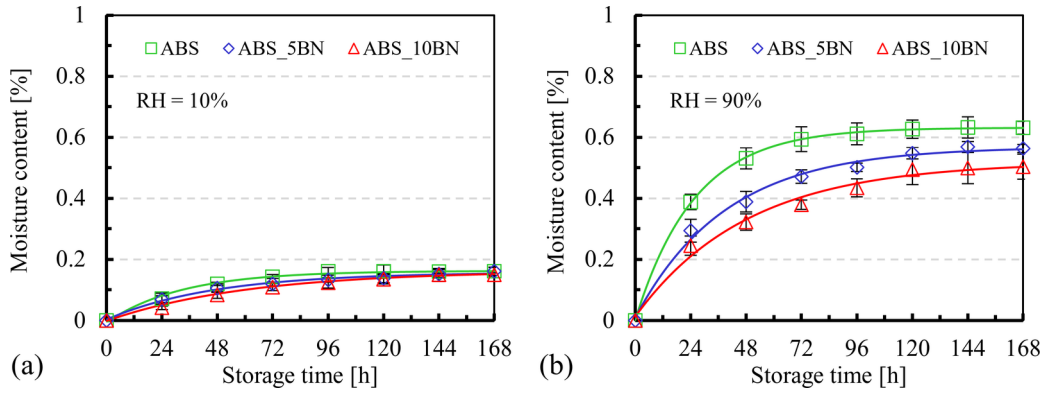

Fig. 3 The moisture content of neat ABS and ABS/BN composite filaments conditioned at 10% (**a**) and 90% (**b**) relative humidity

as physical barriers, hindering the rate of water absorption through blocking moisture diffusion pathways. Similar observations were made in the literature by Dayalan et al. [48], who found that the addition of nanosilica increases the hydrophobicity of basalt/polyester composites, while Alamri et al. [49] analyzed the effect of organoclays, halloysite nanotubes and silicon carbide particles on the water uptake of epoxy, demonstrating that all of the listed fillers decrease the amount of moisture absorbed by the polymer.

3.2 Macro- and microstructure

The macrostructure of the 3D-printed parts was investigated through CT scans, while SEM images were used for microstructural analysis. Figure 4 shows representative cross-sections of ABS and ABS_10BN samples in the X-Y and X-Z planes. In the cross-sections of all neat ABS samples, the individual beads are clearly distinguishable, along with the quasi-triangular raster gap voids in between them, regardless of the filaments' storage conditions. However, it is important to note that the samples prepared from filaments stored at 90% RH contain some intra-bead voids as well, which are assumed to be entrapped steam pockets, pores formed by water evaporation at the elevated processing temperature. Due to their relatively low number, it is suggested that most of the evaporated water was able to escape the heated nozzle, without becoming entrapped inside the deposited beads. Incorporating the BN particles had minimal impact on the cross-section characteristics of the sample when 3D printing was performed using filaments stored at 10% RH. The only noticeable difference was the larger size of the inter-bead voids, which may be attributed to the increased viscosity of the BN-filled material. However, significant changes were detected in the macrostructure when the storage RH of the ABS/BN filament was raised to 90%. The number and size of inter-bead voids decreased markedly, while the cross-sections revealed variations in density, with some regions appearing darker and others lighter. The reduced number of inter-bead voids is likely due to the plasticizing effect of water on the material, which lowers the viscosity, allowing the beads to "spread" better and fuse with each other through a larger interphase. The presence of darker and lighter regions in the CT scans indicates a mixture of dense and porous segments inside the 3D printed parts, although

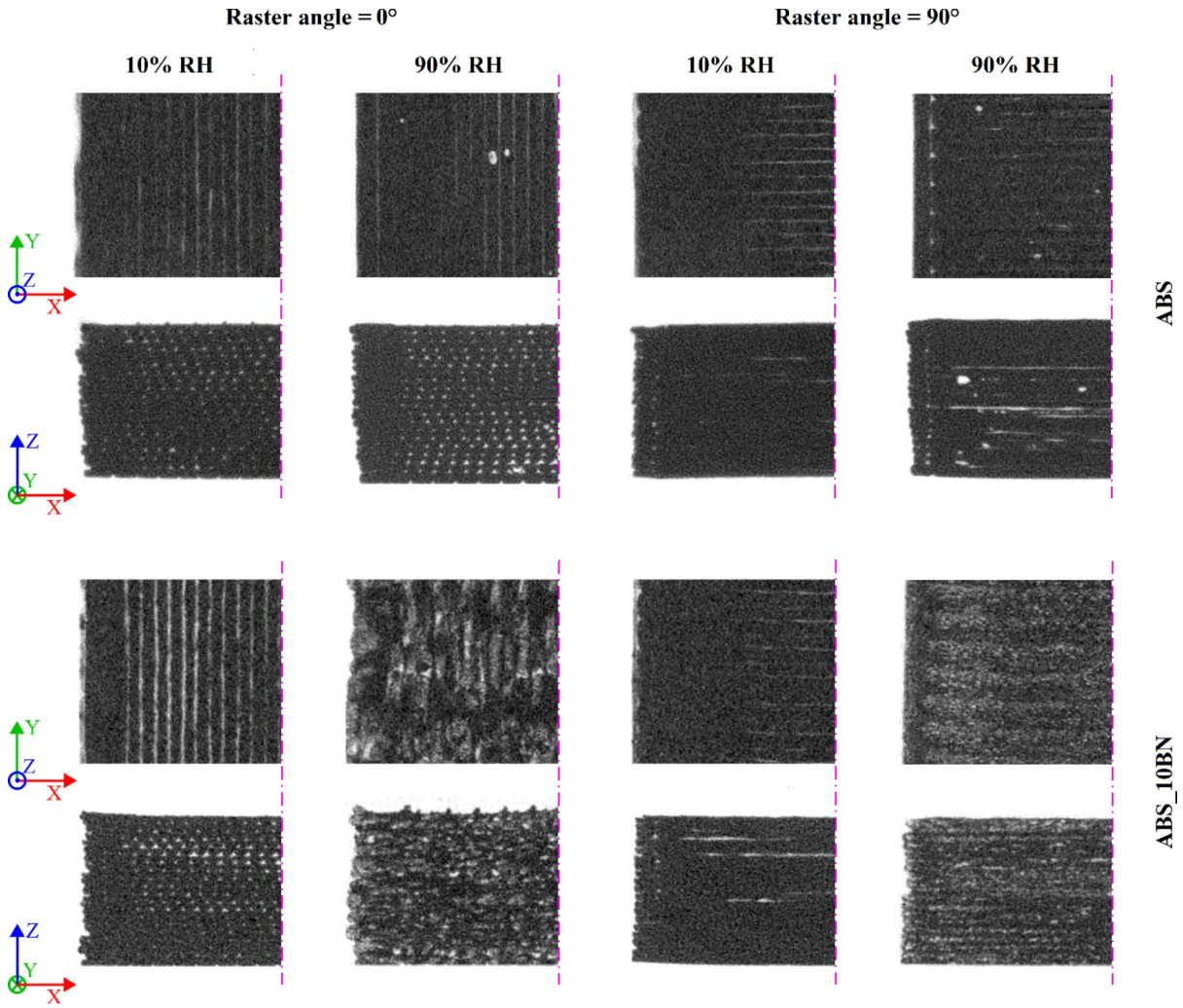

Fig. 4 Characteristic top (X–Y) and side view (X–Z) cross-sections of ABS and ABS_10BN samples based on the CT scans

the resolution of the CT machine did not allow for a more thorough analysis of this phenomenon, which highlighted the necessity for SEM analysis.

Based on the CT scans, the dimensional accuracy of the 3D-printed Charpy specimens was also evaluated by measuring their cross-sectional parameters (width and thickness). Table 1 summarizes the cross-sectional dimensions of the samples. Considering the width of the specimens, it was rather consistent, ranging from 10.53 to 10.63 mm for both ABS and ABS_5BN samples, regardless of raster angle or storage humidity. For ABS_10BN, the raster angle also did not affect the width, unlike storage humidity, which caused significant differences. ABS_10BN specimens 3D-printed using the filament stored at 10% RH had widths of 10.34–10.44 mm (lower than neat ABS), while those prepared from humid filaments measured 10.68–10.72 mm (higher than neat ABS). These changes are most probably due to the altered viscosity of the polymer. Rigid fillers like BN tend to increase the viscosity, and under dry conditions, this resulted in less bead "spreading" and, therefore, decreased sample width. In contrast, in humid filaments, the entrapped moisture is assumed to plasticize the polymer, promoting bead spreading and ultimately leading to a higher width of the 3D-printed specimens.

The thickness of the specimens was primarily affected by the storage humidity conditions of the filaments. Specimens 3D-printed from humid filaments exhibited thickness ~2% greater than those prepared from dry filaments, regardless of composition or raster angle. The increase in thickness can be attributed to volumetric expansion caused by the formation of steam pockets when water evaporated at the processing temperature.

SEM analysis was performed to explore the microstructure of the fabricated ABS and ABS/BN composite specimens, as depicted in Fig. 5. The neat ABS samples exhibited clearly distinguishable beads, with the samples 3D-printed from high-moisture filament also containing intra-bead voids (Fig. 5c, d). These voids, caused by steam entrapment, align

Table 1 Cross-sectional dimensions of the 3D-printed Charpy specimens

Sample	ABS				ABS_5BN				ABS_10BN			
Raster angle	0°		90°		0°		90°		0°		90°	
Storage RH	10%	90%	10%	90%	10%	90%	10%	90%	10%	90%	10%	90%
width [mm]	10.57 ±0.08	10.57 ±0.09	10.53 ±0.06	10.47 ±0.08	10.58 ±0.09	10.60 ±0.11	10.63 ±0.10	10.60 ±0.16	10.34 ±0.30	10.72 ±0.19	10.44 ±0.09	10.68 ±0.17
thickness [mm]	4.04 ±0.03	4.13 ±0.04	4.02 ±0.04	4.18 ±0.05	3.96 ±0.02	4.03 ±0.03	3.91 ±0.03	4.11 ±0.03	3.70 ±0.06	3.98 ±0.05	3.87 ±0.02	3.91 ±0.04

well with the findings of CT scans, where similar pores were identified. The higher resolution provided by SEM reveals additional details about the characteristic microstructure of the BN-filled samples. Apparently, the composites containing 10 vol% BN (ABS_10BN) contain a high number of voids formed through water evaporation when the filament was stored under humid conditions (90% RH). This is rather contradictory considering the lower moisture content of boron nitride-filled composites, as discussed in Sect. 3.1. (Moisture absorption behavior). A plausible explanation for this phenomenon lies in the behavior of BN particles during the 3D-printing process. While their presence hindered moisture absorption, when the filaments were stored in a humid environment, it also seemed to prevent the dissipation of any absorbed water when the ABS/BN composites were heated to melt processing temperature. Evidently, as the temperature rose during the 3D-printing, the absorbed water began to evaporate. However, due to the boron nitride platelets acting as physical barriers, steam became entrapped within the deposited beads. Consequently, in the corresponding samples, the beads are observed to own a characteristic core-shell microstructure, with their core being highly porous due to water evaporation and their shell remaining solid and intact. This core-shell microstructure also explains the lighter and darker regions detected in the CT scans of these specimens, which correspond to the porous and solid areas within the 3D-printed parts.

3.3 Mechanical properties

In order to assess the impact of filament storage humidity, infill orientation, and BN-content on the mechanical properties of MEX 3D-printed objects, tensile tests were performed, with the results shown in Fig. 6. Regarding tensile strength (Fig. 6a, b), neat ABS 3D-printed using a filament storage humidity of 10% RH and a raster angle of 0° exhibited the highest value among the prepared samples (40.5 MPa). The strength of the ABS/BN composites prepared under the same conditions gradually decreased as BN content increased, bottoming at 34.1 MPa with 10 vol% hexagonal BN particles. The reduction in strength can be attributed to poor matrix/reinforcement interactions due to differences in surface chemistry between the polymer and the ceramic filler. According to the literature [50], composites filled with inorganic additives, where the compatibility between the components is limited, typically exhibit reduced strength. The trends were similar for samples 3D-printed with a raster angle of 90°. However, the absolute values of strength were considerably lower in that case; neat ABS exhibited a tensile strength of 36.7 MPa, while ABS_5BN and ABS_10BN showed 23.8 MPa and 22.3 MPa, respectively. These discrepancies between strength values for different infill angles

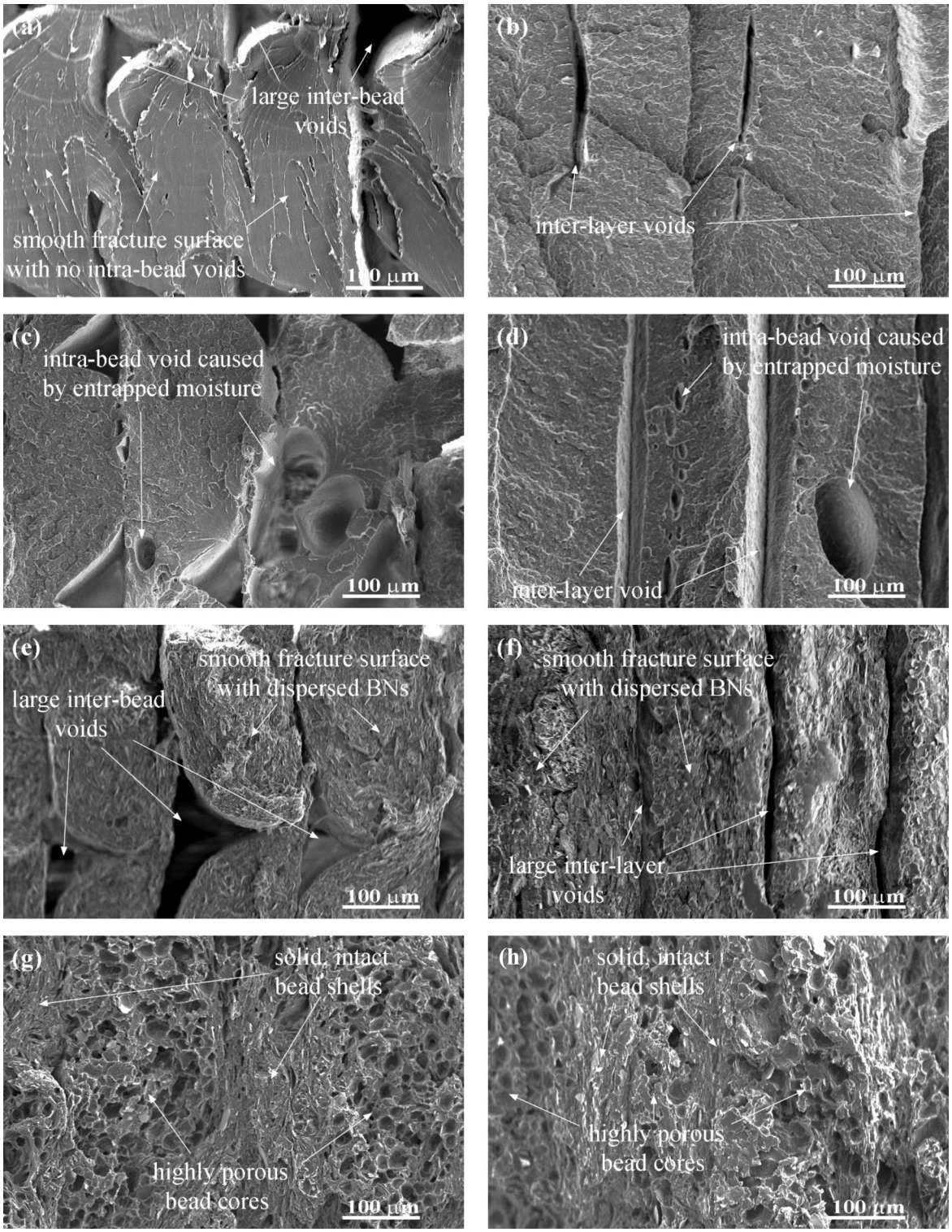

Fig. 5 SEM images of the cross-sections of samples (**a**) ABS (10% RH, 0° RA), (**b**) ABS (10% RH, 90° RA), (**c**) ABS (90% RH, 0° RA), (**d**) ABS (90% RH, 90° RA), (**e**) ABS_10BN (10% RH, 0° RA), (**f**) ABS_10BN (10% RH, 90° RA), (**g**) ABS_10BN (90% RH, 0° RA), (**h**) ABS_10BN (90% RH, 90° RA)

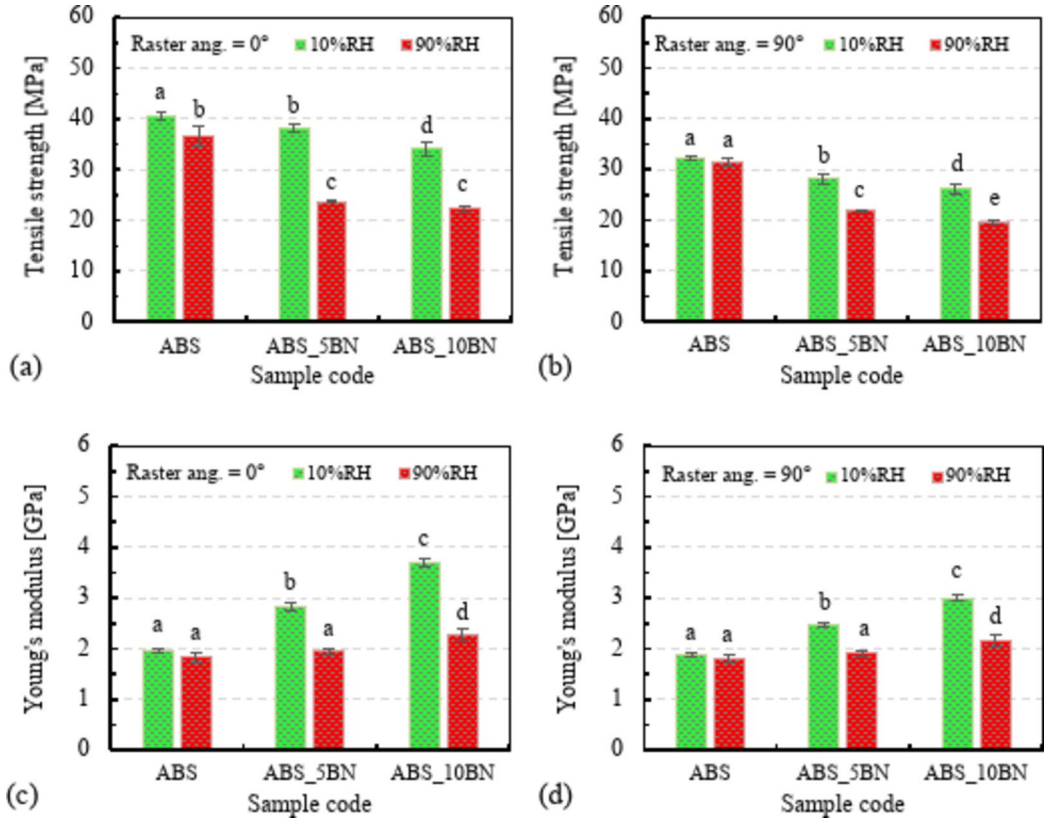

Fig. 6 Tensile strength (**a**, **b**) and Young's modulus (**c**, **d**) of ABS and its BN-filled composites 3D-printed with a 0° and 90° raster angle at different filament storage humidity values. The different letters (a, b, c, d, e) above the columns indicate significant differences among composites according to Tukey's HSD test ($p < 0.05$)

can be attributed to differences in failure modes that occur during the tensile testing, namely inter-bead bond failure and trans-bead failure. In specimens 3D printed with a raster angle of 90°, the material was stretched perpendicular to the bead deposition direction, resulting in inter-bead fusion bond failure. In such cases, bead-to-bead adhesion majorly affects tensile strength, as the inter-bead fusion bonds between adjacent beads must withstand most of the applied load rather than the ABS or ABS/BN material itself. Due to their oval cross-section, the beads are not fully fused with the neighboring ones, typically leading to a lower tensile strength, as reported in previous studies [40, 51].

Increasing the environmental humidity where the feedstock was stored resulted in a decrease in tensile strength, regardless of BN-content or infill orientation. The rate of reduction, however, obviously varied. At a 0° raster angle, the reduction in strength was 10%, 37%, and 35% for samples ABS, ABS_5BN and ABS_10BN, respectively. Meanwhile, it was only 2%, 22%, and 24% when the infill orientation was 90°. Evidently, 3D-printed parts were less affected by filament moisture when inter-bead failure was the typical failure mode and more sensitive when trans-bead failure prevailed. This can be ascribed to the fact that void formation did not directly influence the bead bond quality, as steam entrapment typically occurred within the interior of the beads. This is in good agreement with the observations made based on the SEM images showing that the interfaces between the beads are rather intact, while the resulting morphology of the bulk material within the beads was affected by the moisture content of the filament. The formation of voids due to the evaporation of water significantly weakened the load bearing capacity of the material, particularly in hexagonal BN-filled composites, where water was not able to evaporate. Generally, higher porosity leads to lower strength, as there is less solid material to carry and distribute the mechanical load.

In contrast to strength, Young's modulus (Fig. 6c, d) increased as a function of BN-content regardless of storage humidity or infill orientation. The reason Young's modulus showed an opposite trend from tensile strength with BN-loading is that the former is less influenced by the quality of the chemical bonds between the components. Even though the interfacial bonding between ABS and BN may not be strong enough to enable load transfer under large strains, it is still sufficient in the early elastic region, where modulus is calculated. Therefore, the characteristic features of the additives are more determinant in this respect [29, 52]. Ceramic fillers, such as BN, are quite rigid, hindering the mobility

of ABS chain molecules and ultimately leading to higher stiffness. Interestingly, the degree of improvement greatly depended on the variables (infill orientation and filament moisture content). Neat ABS exhibited a modulus of 1.95 GPa when 3D-printed using an infill orientation parallel to the tensile load (0°) and 1.87 GPa when perpendicular (90°) to that. The most optimal results were once again found for the samples prepared with a filament of lower moisture content and an infill orientation parallel to the tensile load (raster angle = 0°). The ABS_10BN specimens fabricated this way outperformed all other samples with their Young's modulus of 3.7 GPa. It is important to note that this improvement is even higher than that previously observed for compression molded bulk samples of identical composition, where the modulus of ABS increased from 1.73 GPa to 3.09 GPa when filled with 10 vol% BN [29]. The increased modulus of neat ABS is assumed to be due to the intensive molecular orientation induced by 3D printing in the direction of the tensile load when using a 0° infill. Similarly, the BN platelets are likely aligned in the same direction, resulting in more effective reinforcement. As expected, modulus values were lower for samples with a raster angle of 90° compared to the ones with 0°, which is due to the same reason that tensile strength also decreased, namely the impact of bead-interphase bonds. Interestingly, this trend was observed only for samples prepared of low-moisture feedstocks. For filaments stored at 90% RH, the modulus values of samples with specific compositions were nearly identical, regardless of infill orientation. It is worth noting that, despite the formation of a porous macrostructure, the modulus still improved slightly with increasing BN-content, suggesting that the loss presumably caused by the presence of voids was overcompensated by the reinforcement effect of BN particles.

The results of the Charpy impact tests are presented in Fig. 7. Neat ABS exhibited the highest toughness, with an impact strength of 61.7 kJ/m^2 and 49.4 kJ/m^2 when 3D-printed using a raster angle of 0°, with filaments stored at 10% and 90% RH, respectively. Accordingly, increasing the humidity in the climate chamber led to a relative reduction of 20%. With increasing hexagonal BN content, the toughness of ABS gradually decreased, which can be attributed to the limited adhesion between the polymer and the reinforcement. The poorly bonded ceramic particles likely acted as stress concentration sites, promoting the development of microcracks upon impact loading and ultimately reducing the impact toughness of the composites. The difference between the specimens 3D-printed from dry and humid filaments was more pronounced in the case of BN-reinforced composites, with relative reductions of 45% and 34% for samples ABS_5BN and ABS_10BN, respectively. This is assumed to be the consequence of the large number of steam voids in these materials, compromising the structural integrity and thereby reducing the impact resistance of the 3D-printed parts. The impact strength of the specimens prepared with a raster angle of 90° was significantly lower compared to the ones printed with 0° due to the weak bead-interphase bonds. For the same reason, the impact of storage humidity was also less significant in this case. The reduction for neat ABS when increasing the environmental humidity to 90% was 14%, while it was 24% and 11% for samples ANS_5BN and ABS_10BN, respectively, which is in good agreement with the tensile tests' results.

3.4 Thermomechanical behavior

The experiments conducted with the use of DMA confirmed the results of tensile tests regarding the modulus of the samples. Accordingly, the storage modulus (*E'*), which reflects the stiffness, was rather similar for all neat ABS specimens (Fig. 8a), with slightly higher values for those 3D-printed using filaments stored under lower RH conditions. Specifically, ABS 3D-printed using a 0° raster angle and a filament stored at 10% RH owned a storage modulus of 1600 MPa at 50 °C while the one manufactured with an infill orientation

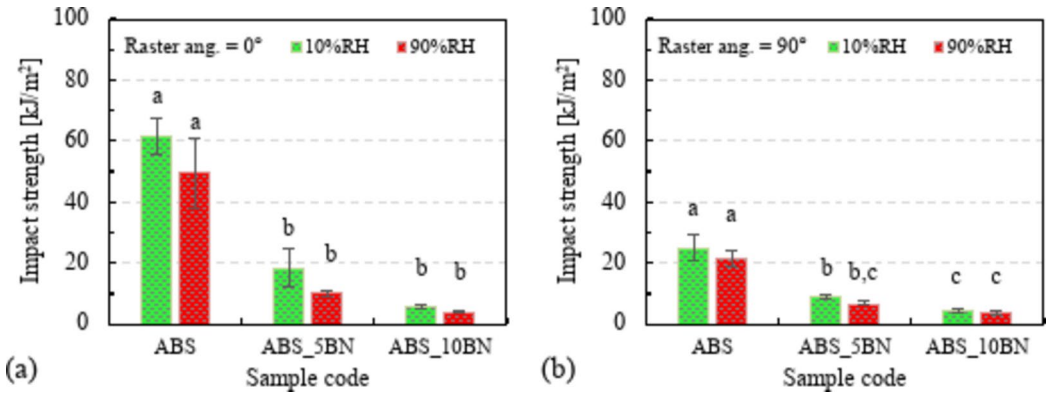

Fig. 7 Charpy impact strength of ABS and its BN-filled composites 3D-printed with a 0° (**a**) and 90° (**b**) raster angle at different filament storage humidity values. The different letters (a, b, c) above the columns indicate significant differences among composites according to Tukey's HSD test ($p < 0.05$)

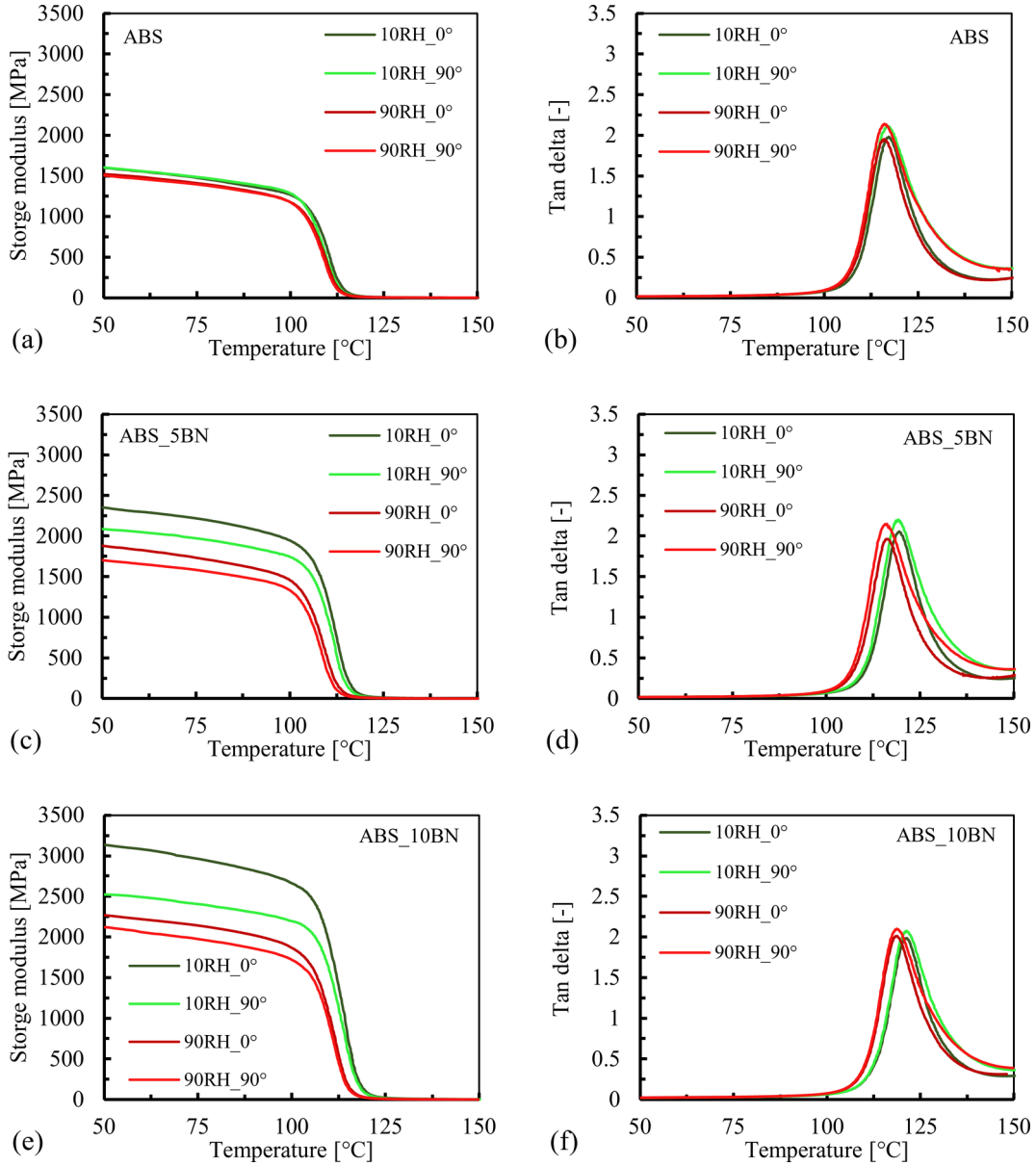

Fig. 8 Storage modulus and loss factor as a function of temperature for ABS (**a**, **b**), ABS_5BN (**c**, **d**), and ABS_10BN (**e**, **f**) samples at different filament storage humidity values and printing infill orientations

of 90° exhibited 1601 MPa at the same temperature. In the case of 90% filament storage humidity, these values were slightly lower: 1521 MPa for the 0° raster angle and 1506 MPa for the 90°. Regarding the infill orientation, it is extensively reported in the literature that the printing angle has a relatively significant impact on the dynamic mechanical properties of MEX 3D-printed parts. A raster angle of 0° (infill parallel to the length of the specimen) yields the highest storage modulus (*E'*) and the lowest loss modulus (*E''*) and loss factor (*tan δ*) [53, 54]. Conversely, increasing the raster angle results in a higher loss modulus and loss factor, although at the cost of storage modulus. This suggests that ABS 3D-printed at 0° raster angle has more load-storing potential, while ABS 3D-printed at 90° is more prone to dissipate energy rather than storing it. When hexagonal BN particles were incorporated into the polymer, the modulus of the samples increased considerably, particularly below the glass transition temperature (T_g). The T_g of the samples, taken as the peak of loss factor curves, increased with the introduction of hexagonal BN particles, as can be observed in the *tan δ* plots (Fig. 8b, d, f). In the case of samples fabricated with 10% filament storage RH and 0° raster angle, the T_g was 117.3 °C, 119.5 °C, and 121.4 °C for ABS, ABS_5BN, and ABS_10BN, respectively. Such an increase in glass transition temperature often occurs when rigid inorganic fillers are incorporated into the polymer as they act

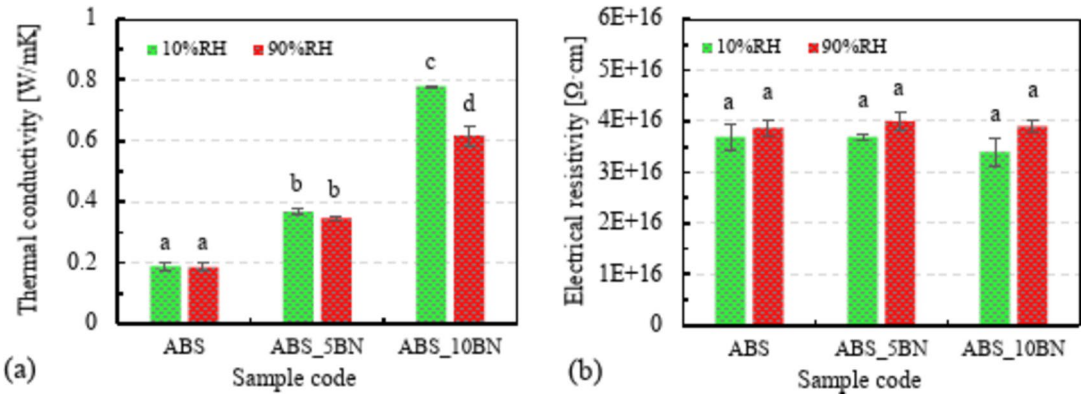

Fig. 9 Thermal conductivity (**a**) and electrical resistivity (**b**) of ABS and its BN-filled composites 3D-printed at different filament storage humidity values. The different letters (a, b, c, d) above the columns indicate significant differences among composites according to Tukey's HSD test ($p < 0.05$)

as a physical hindrance, thereby restricting the mobility of polymer chain molecules. Similar phenomena have been widely reported in the literature for various ceramic particle-filled polymer composites [55, 56]. The trend of the storage modulus curves was consistent across the ABS_5BN and ABS_10BN composites as well, with the highest modulus values measured under the conditions of 10% filament storage RH and 0° raster angle. The lowest values were always found in the case of 90% storage RH and a raster orientation perpendicular to the length of the specimen (90°). Major differences were observed in the *E'* plots of ABS_5BN and ABS_10BN composites when the storage humidity of filaments was increased from 10 to 90%. At 50 °C, the storage modulus of ABS_5BN when 3D printed with a raster angle of 0° decreased from 2353 MPa to 1881 MPa when the storage RH was increased (a difference of 473 MPa), which is more than five times as much as observed for neat ABS. In the case of ABS_10BN, the reduction was even larger: 867 MPa (from 3136 MPa to 2269 MPa). The decline in storage modulus with increasing filament moisture can be attributed to the formation of voids, which intensified with higher BN content, as corroborated by the CT and SEM analyses. This is also in good agreement with the previously discussed mechanical test results. The T_g of the samples was also affected by filament moisture content. Increasing the RH in the storage chamber from 10 to 90% resulted in a drop of ~1 °C, ~3 °C, and ~3 °C for samples ABS, ABS_5BN, and ABS_10BN, respectively. This reduction in glass transition is likely due to the increased porosity in the samples, which reduces the effective polymer mass that absorbs thermal energy during heating. Consequently, with less bulk mass, less energy is required to make the chain molecules mobile.

3.5 Conductivity properties

The results of thermal conductivity and electrical resistivity measurements are presented in Fig. 9. Based on the LFA measurements, neat ABS exhibited the lowest thermal conductivity among the fabricated samples: 0.188 W/mK when 3D-printed using the filament stored at 10% RH and only a slightly lower value of 0.185 W/mK when prepared using the filament maintained at 90% RH. The relatively small difference is reasonable, considering that neat ABS developed the fewest voids when using the more humid feedstock, which could have compromised thermal conductivity due to the low conductivity of air (~ 0.03 W/mK). The introduction of hexagonal BN particles into the polymer obviously increased its conductivity. The ABS_5BN material exhibited thermal conductivities of 0.368 W/mK and 0.346 W/mK, with the specimens 3D-printed with the filament of higher moisture content proving inferior once again. Note that these values are still considerably higher than those measured for ABS/BN composites of the same composition [29] prepared via compression molding (0.275 W/mK), which is unexpected considering the inherent voids found in 3D-printed parts. This discrepancy, favoring the 3D-printed objects, may be attributed to the differences in the alignment of the BN platelets. Hexagonal BN has a highly anisotropic thermal conductivity ascribed to its layered structure, with in-plane conductivity ranging between 220 W/mK and 600 W/mK [57], while through-plane conductivity is only ~2.5 W/mK [58]. Inside the compression molded samples, the hexagonal BN particles are predominantly aligned perpendicularly to the direction of LFA measurement, making the through-plane conductivity the dominant conductivity mode. In contrast, 3D printing the specimens with the infill strategy used in this study results in BN platelet orientations where the probability of being aligned parallel or perpendicular to the measurement direction is more evenly

distributed. The highest thermal conductivity was measured for ABS_10BN when 3D printing was carried out with the filament stored at 10% RH, with a value of 0.778 W/mK. However, this sample also experienced the most significant drop in thermal conductivity when the filament storage humidity was increased to 90%, falling to 0.617 W/mK. The greater loss at higher BN is likely due to the more intensive formation of voids caused by water entrapment during the processing, which ultimately disrupted the conductive pathways in the 3D-printed parts. Additionally, altered filler alignment – also influenced by the void formation – may have a further impact on thermal conductivity.

The electrical resistivity of all samples was found to be in the relatively small range of 3.7×10^{16} Ω·cm to 3.9×10^{16} Ω·cm. Similar to the thermal conductivity results, these values were significantly higher than those previously measured for bulk ABS/BN samples of the same composition fabricated using compression molding instead of 3D printing (1.1×10^{12} Ω·cm to 1.6×10^{12} Ω·cm as BN content increased) [29]. Unlike thermal conductivity, BN's electrical resistivity is rather isotropic with excellent resistivity in all directions, typically measuring 10^{13}–10^{15} Ω·cm [59], making it an effective electrical insulator. Consequently, since particle alignment is not expected to influence the resistivity, the reason for the multiple magnitudes of differences observed between 3D printing and compression molding can be attributed to the following two factors: (i) the inherent presence of air voids in 3D-printed structures, which act as insulators, with air resistivity being in the range of 10^{13}–10^{16} Ω·cm [60]; and (ii) the uneven surface of the 3D-printed specimens, which prevents perfect contact with the measuring device's solid surface. Overall, it can be concluded that the addition of hexagonal BN does not significantly affect the resistivity of ABS. Meanwhile, increasing the filament storage humidity led to a slight increase in resistivity regardless of the sample composition, which can be attributed to the formation of voids.

4 Conclusions

In this study, acrylonitrile-butadiene-styrene/hexagonal boron nitride composites were prepared for heat sink applications, and their processability was investigated through material extrusion-based additive manufacturing, focusing on the influence of the feedstocks' moisture content. In addition to filament moisture content, the effect of infill raster angle on the properties of the 3D-printed objects was also examined. The BN content of the prepared samples was 0, 5, and 10 vol%, with filaments stored at 10% and 90% ambient humidity, and the infill raster angles used were 0° and 90°. Water uptake measurement revealed that hexagonal BN, being a hydrophobic ceramic material, effectively hindered the moisture absorption of ABS. However, it did not reduce the moisture sensitivity of the filaments during processing. On the contrary, BN-containing materials exhibited extensive void formation during 3D printing, as the BN particles prevented water from dissipating, leading to steam entrapment in these materials, as evidenced by computed tomographic and scanning electron microscopic analyses. The entrapped steam intensively promoted void development within the deposited beads, facilitating the formation of a highly porous microstructure. Consequently, the mechanical properties, i.e., tensile strength, Young's modulus, and impact strength of the ABS/BN composites deteriorated significantly when humid filaments were used. The reduction in these properties was most pronounced in the case of 0° raster angle, and it was less severe for parts 3D printed with a 90° infill orientation due to their inherently weaker structure, ascribed to the role of bead-interphase bonds in the load-bearing. Dynamic mechanical analysis revealed a slight decrease in glass transition temperature with increasing raster angle and filament storage humidity. The thermal conductivity of ABS improved significantly with BN addition and only slightly deteriorated as a consequence of storage humidity, with the loss being ascribed to the presence of voids. The electrical conductivity was barely influenced by BN content and it only slightly deteriorated with increased filament moisture.

Overall, considering the investigated properties, it is safe to assume that preliminary drying of ABS/BN composites, before being MEX 3D-printed is clearly beneficial. In the case, when the use of dry filament is not feasible, a moderate BN concentration in ABS might offer a balance between thermal conductivity and mechanical properties.

Acknowledgements Project no. TKP2021-NVA-23 has been implemented with the support provided by the Ministry of Culture and Innovation of Hungary from the National Research, Development and Innovation Fund, financed under the TKP2021-NVA funding scheme. L. Lendvai is grateful for János Bolyai Research Scholarship of the Hungarian Academy of Sciences. This research was supported by the ÚNKP-23-5-SZE-112 New National Excellence Program of the Ministry for Culture and Innovation from the source of the National Research, Development and Innovation Fund.

Author contributions Each author participated sufficiently in the work. L.L. and S.K.J. produced the samples. L.L., I.F and D.R. performed the analyses. L.L. and A.P. wrote the main manuscript text. All authors reviewed the manuscript.

Funding Open access funding provided by Széchenyi István University (SZE).

Data availability Data will be made available on request.

Declarations

Conflict of interest The authors have no competing interests as defined by Springer, or other interests that might be perceived to influence the results and/or discussion reported in this paper.

References

1. A. Glogowsky, M. Korger, M. Rabe, Influence of print settings on conductivity of 3D printed elastomers with carbon-based fillers. Progress Additive Manuf. **9**, 791–803 (2024)
2. C. Zhai, J. Wang, Y. Tu, G. Chang, X. Ren, C. Ding, Robust optimization of 3D printing process parameters considering process stability and production efficiency. Additive Manuf. **71**, 103588 (2023)
3. A.A. Desai, S. Dnyandev Patil, P.H. Yadav, A. Kekare, Design, analysis, and development of additive manufacturing by using FDM technique with dual nozzle assembly. Mater. Today: Proc. **77**, 619–626 (2023)
4. M.-H. Hsueh, C.-J. Lai, S.-H. Wang, Y.-S. Zeng, C.-H. Hsieh, C.-Y. Pan, W.-C. Huang, Effect of printing parameters on the thermal and mechanical properties of 3D-Printed PLA and PETG, using fused deposition modeling. Polym. (Basel). **13**, 1758 (2021)
5. M. Daly, M. Tarfaoui, M. Chihi, C. Bouraoui, FDM technology and the effect of printing parameters on the tensile strength of ABS parts. Int. J. Adv. Manuf. Technol. **126**, 5307–5323 (2023)
6. M. Kováčová, A. Vykydalová, Z. Špitálský, Polycaprolactone with glass beads for 3D printing filaments. Processes. **11**, 395 (2023)
7. N. Vidakis, M. Petousis, E. Velidakis, M. Liebscher, V. Mechtcherine, L. Tzounis, On the strain rate sensitivity of fused filament fabrication (FFF) processed PLA, ABS, PETG, PA6, and PP thermoplastic polymers. Polym. (Basel). **12**, 2924 (2020)
8. N. Divakaran, A. Y, A. Mohapatra, S. Mohanty, Material extrusion-based 3D printed capacitor optimization: enhancing performance with ZnO and Cu-CNT reinforced ABS composites. Appl. Mater. Today. **40**, 102363 (2024)
9. N. Sabahi, E. Farajzadeh, I. Roohani, C.H. Wang, X. Li, Material extrusion 3D printing of polyether-ether-ketone scaffolds based on triply periodic minimal surface designs: A numerical and experimental investigation. Appl. Mater. Today. **39**, 102262 (2024)
10. Y. Guldorum, M.N. Danisik, M.K. Zia, N. Aldemir, S. Ulag, L. Bicer, E. Kaya, A. Sahin, G.B. Tinaz, O. Gunduz, Development of 3D-printed PCL scaffolds enriched with hyaluronic acid and Gallic acid for wound dressing. Emergent Mater (2025)
11. S. Li, B. Fang, Y. Wang, F. Zou, J. Zhao, H. Zhang, J. Guo, Z. Wang, J. Xu, Three-dimensional printing of Boron nitride platelets/polylactic acid composites: achieving enhanced through plane thermal conductivity and decent mechanical properties. Polym. Compos. **46**, 4605–4613 (2025)
12. Z. García-Hernández, O. Molina-Ramírez, J.E. Rivera-Salinas, I. Sifuentes-Nieves, P. González-Morones, Hernández-Hernández, Boron nitride: the key material in polymer composites for electromobility. Polym. Compos. **46**, 1976–2029 (2025)
13. M. Hassan, M.A. Gondal, E. Cevik, T.F. Qahtan, A. Bozkurt, M.A. Dastageer, High performance pliable supercapacitor fabricated using activated carbon nanospheres intercalated into Boron nitride nanoplates by pulsed laser ablation technique. Arab. J. Chem. **13**, 6696–6707 (2020)
14. W. Wu, M. Zheng, K. Lu, F. Liu, Y.-H. Song, M. Liu, Z.-M. Dang, Thermally conductive composites based on hexagonal Boron nitride nanosheets for thermal management: fundamentals to applications. Compos. Part A: Appl. Sci. Manufac. **169**, 107533 (2023)
15. Z. Wang, X. Wang, Z. Zhang, L. Liang, Z. Zhao, J. Shi, Preparation of a 3D BN network structure by a salt-template-assisted method filled with epoxy resin to obtain high thermal conductivity nanocomposites. Polym. Compos. **44**, 3610–3621 (2023)
16. Z. Wang, X. Wang, Z. Zhang, L. Liang, Z. Zhao, J. Shi, Highly thermally conductive polymer composite enhanced by constructing a dual thermal conductivity network. Polym. Compos. **44**, 5734–5745 (2023)
17. S. Bagatella, A. Cereti, F. Manarini, M. Cavallaro, R. Suriano, M. Levi, Thermally conductive and electrically insulating Polymer-Based composites heat sinks fabricated by fusion deposition modeling. Polym. (Basel). **16**, 432 (2024)
18. M. Bragaglia, F.R. Lamastra, P. Russo, L. Vitiello, M. Rinaldi, F. Fabbrocino, F. Nanni, A comparison of thermally conductive polyamide 6-boron nitride composites produced via additive layer manufacturing and compression molding. Polym. Compos. **42**, 2751–2765 (2021)
19. X. Wu, W. Liu, F.-. Shi, L. Yang, C. Zhang, Constructing three-dimensional Boron nitride network for highly thermally conductive epoxy resin composites. Polym. Compos. **43**, 1711–1717 (2022)
20. A. KarimzadGhavidel, T.T. Opoz, M. Mahdavinia, G. Kiani, M. Moradi, Achieving exceptional mechanical and thermal properties in ABS/MWCNTs nanocomposites with minimal CNT loading via electromechanical dispersion technique. *Polymer Composites*, n/a
21. Y. Ouyang, F. Ding, L. Bai, X. Li, G. Hou, J. Fan, F. Yuan, Design of network Al2O3 spheres for significantly enhanced thermal conductivity of polymer composites. Compos. Part A: Appl. Sci. Manufac. **128**, 105673 (2020)
22. D. Liu, C. Ma, H. Chi, S. Li, P. Zhang, P. Dai, Enhancing thermal conductivity of polyimide composite film by electrostatic self-assembly and two-step synergism of Al2O3 microspheres and BN nanosheets. RSC Adv. **10**, 42584–42595 (2020)
23. M.W. Akhtar, J.S. Kim, M.A. Memon, M.Y. Khan, M.M. Baloch, Surface modification of magnesium oxide/epoxy composites with significantly improved mechanical and thermal properties. J. Mater. Sci.: Mater. Electron. **32**, 15307–15316 (2021)
24. A. Khan, M. Puttegowda, P. Jagadeesh, H.M. Marwani, A.M. Asiri, A. Manikandan, A.A. Parwaz Khan, G.M. Ashraf, S.M. Rangappa, S. Siengchin, Review on nitride compounds and its polymer composites: a multifunctional material. J. Mater. Res. Technol. **18**, 2175–2193 (2022)
25. Z. Lule, J. Kim, Thermally conductive and highly rigid polylactic acid (PLA) hybrid composite filled with surface treated alumina/nano-sized aluminum nitride. Compos. Part A: Appl. Sci. Manufac. **124**, 105506 (2019)
26. G. Wu, Y. Wang, K. Wang, A. Feng, The effect of modified AlN on the thermal conductivity, mechanical and thermal properties of aln/polystyrene composites. RSC Adv. **6**, 102542–102548 (2016)
27. M. Qian, P. Song, Z. Qin, S. Yan, L. Zhang, Mechanically robust and abrasion-resistant polymer nanocomposites for potential applications as advanced clearance joints. Compos. Part A: Appl. Sci. Manufac. **126**, 105607 (2019)

28. D. Shen, M. Wang, Y. Wu, Z. Liu, Y. Cao, T. Wang, X. Wu, Q. Shi, K.W.A. Chee, W. Dai, H. Bai, D. Dai, J. Lyu, N. Jiang, C.-T. Lin, J. Yu, Enhanced thermal conductivity of epoxy composites with core-shell SiC@SiO2 nanowires. High. Voltage. **2**, 154–160 (2017)
29. L. Lendvai, T. Singh, D. Rigotti, A. Pegoretti, Thermally conductive and electrically resistive acrylonitrile butadiene styrene (ABS)/boron nitride composites: optimal design using a multi-criteria decision-making approach. J. Mater. Res. Technol. **26**, 8776–8788 (2023)
30. K. Li, Y. Liu, S. Wang, X. Jin, W. Li, W. Gan, S. Song, Construction of 3D framework of BN and silica with advanced thermal conductivity of epoxy composites. J. Polym. Res. **30**, 219 (2023)
31. J. Kovacs, A. Suplicz, Thermally conductive polymer compounds for injection moulding: the synergetic effect of hexagonal boron-nitride and Talc. J. Reinf. Plast. Compos. **32**, 1234–1240 (2013)
32. F. You, X. Ke, G. Tang, X. Yan, R. Chen, X. Jiang, C. Yao, Enhanced thermal conductivity in Boron nitride incorporated polyethylene/polymethyl methacrylate composites via double percolation structure. Polym. Compos. **45**, 4550–4560 (2024)
33. P. Guo, Q. Liu, X. Zhang, J. Liang, Q. Li, K. Zheng, W. Wu, Temperature-sensitive polymer composite-enabled all-printed flexible temperature sensors for safety monitoring. Compos. Part. B: Eng. **300**, 112474 (2025)
34. S. Gul, S. Arican, M. Cansever, M. Yildiz, B. Saner, Okan, Dimension effect on thermal conductivity of hexagonal Boron nitride/titanium dioxide reinforced hybrid PEEK composites developed with a scalable compounding approach. Polym. Compos. **44**, 8669–8682 (2023)
35. M.T. Birosz, M. Andó, Effect of infill pattern scaling on mechanical properties of FDM-printed PLA specimens. Progress Additive Manuf. **9**, 875–883 (2024)
36. D. Croccolo, M. De Agostinis, S. Fini, M. Mele, G. Olmi, G. Campana, Effects of infill temperature on the tensile properties and warping of 3D-printed polylactic acid. Progress Additive Manuf. **9**, 919–934 (2024)
37. L. Lendvai, I. Fekete, D. Rigotti, A. Pegoretti, Experimental study on the effect of filament-extrusion rate on the structural, mechanical and thermal properties of material extrusion 3D-printed polylactic acid (PLA) products. Progress Additive Manuf. **10**, 619–629 (2025)
38. M. Srikanth, A.T. Mathew, R.K. Bhagchandani, Model performance evaluation of build time using geometric shape complexity and process parameters in material extrusion. Additive Manuf. **91**, 104337 (2024)
39. A.P. Agrawal, V. Kumar, J. Kumar, P. Paramasivam, S. Dhanasekaran, L. Prasad, An investigation of combined effect of infill pattern, density, and layer thickness on mechanical properties of 3D printed ABS by fused filament fabrication. Heliyon **9**, e16531 (2023)
40. J.M. Chacón, M.A. Caminero, E. García-Plaza, P.J. Núñez, Additive manufacturing of PLA structures using fused deposition modelling: effect of process parameters on mechanical properties and their optimal selection. Mater. Design. **124**, 143–157 (2017)
41. O. Ulkir, I. Ertugrul, S. Ersoy, B. Yağımlı, The effects of printing temperature on the mechanical properties of 3D-Printed acrylonitrile butadiene styrene. Appl. Sci. **14**, 3376 (2024)
42. L. Fang, Y. Yan, O. Agarwal, S. Yao, J.E. Seppala, S.H. Kang, Effects of environmental temperature and humidity on the geometry and strength of polycarbonate specimens prepared by fused filament fabrication. Materials. **13**, 4414 (2020)
43. A. Hamrol, B. Góralski, R. Wichniarek, The influence of moisture absorption and desorption by the ABS filament on the properties of additively manufactured parts using the fused deposition modeling method. Materials. **17**, 1988 (2024)
44. S.N.A.M. Halidi, J. Abdullah, Moisture effects on the ABS used for fused deposition modeling rapid prototyping machine. 2012 IEEE symposium on humanities, science and engineering research (2012), pp. 839–843
45. D. Laumann, D. Spiehl, E. Dörsam, Influence of printing material moisture on part adhesion in fused filament fabrication 3D printing. J. Adhes. **100**, 380–394 (2024)
46. R. Wichniarek, A. Hamrol, W. Kuczko, F. Górski, M. Rogalewicz, ABS filament moisture compensation possibilities in the FDM process. CIRP J. Manufact. Sci. Technol. **35**, 550–559 (2021)
47. L. Lendvai, I. Fekete, S.K. Jakab, G. Szarka, K. Verebélyi, B. Iván, Influence of environmental humidity during filament storage on the structural and mechanical properties of material extrusion 3D-printed poly(lactic acid) parts. Results Eng. 103013 (2024)
48. P. Dayalan, P.A. Mahanwar, Effect of nano silica on mechanical and water absorption properties of basalt/polyester hybrid composite with glass/hemp. J. Polym. Res. **30**, 341 (2023)
49. H. Alamri, I.M. Low, Effect of water absorption on the mechanical properties of nano-filler reinforced epoxy nanocomposites. Mater. Design. **42**, 214–222 (2012)
50. S.K. Nayak, A. Satapathy, Development and characterization of polymer-based composites filled with micro-sized waste marble dust. Polym. Polym. Compos. **29**, 497–508 (2021)
51. Y. Tang, J. Xiao, T. Ding, H. Liu, M. Zhang, J. Zhang, Trans-layer and inter-layer fracture behavior of extrusion-based 3D printed concrete under three-point bending. Eng. Fract. Mech. **296**, 109836 (2024)
52. L. Lendvai, F. Ronkay, G. Wang, S. Zhang, S. Guo, V. Ahlawat, T. Singh, Development and characterization of composites produced from recycled polyethylene terephthalate and waste marble dust. Polym. Compos. **43**, 3951–3959 (2022)
53. S. Wang, Y. Ma, Z. Deng, S. Zhang, J. Cai, Effects of fused deposition modeling process parameters on tensile, dynamic mechanical properties of 3D printed polylactic acid materials. Polym. Test. **86**, 106483 (2020)
54. O.A. Mohamed, S.H. Masood, J.L. Bhowmik, Characterization and dynamic mechanical analysis of PC-ABS material processed by fused deposition modelling: an investigation through I-optimal response surface methodology. Measurement. **107**, 128–141 (2017)
55. S.S. Samsudin, M.S. Abdul Majid, M.R. Mohd Jamir, A.F. Osman, M. Jaafar, H.A. Alshahrani, Physical, Thermal Transport, and Compressive Properties of Epoxy Composite Filled with Graphitic- and Ceramic-Based Thermally Conductive Nanofillers. Polymers (Basel) **14**, 1014 (2022)
56. L. Lendvai, D. Rigotti, Thermal and thermomechanical properties of Boron nitride-filled acrylonitrile butadiene styrene (ABS) composites. Acta Technica Jaurinensis. **16**, 123–128 (2023)
57. C. Yuan, J. Li, L. Lindsay, D. Cherns, J.W. Pomeroy, S. Liu, J.H. Edgar, M. Kuball, Modulating the thermal conductivity in hexagonal Boron nitride via controlled Boron isotope concentration. Commun. Phys. **2**, 43 (2019)
58. C. Pan, J. Zhang, K. Kou, Y. Zhang, G. Wu, Investigation of the through-plane thermal conductivity of polymer composites with in-plane oriented hexagonal Boron nitride. Int. J. Heat Mass Transf. **120**, 1–8 (2018)
59. C. Steinborn, M. Herrmann, U. Keitel, A. Schönecker, J. Räthel, D. Rafaja, J. Eichler, Correlation between microstructure and electrical resistivity of hexagonal Boron nitride ceramics. J. Eur. Ceram. Soc. **33**, 1225–1235 (2013)
60. E. Seran, M. Godefroy, N. Renno, H. Elliott, Variations of electric field and electric resistivity of air caused by dust motion. J. Geophys. Research: Space Phys. **118**, 5358–5368 (2013)